nature immunology

Fibroblastic reticular cells in lymph nodes regulate the homeostasis of naive T cells

Alexander Link[1,4], Tobias K Vogt[1,4], Stéphanie Favre[1], Mirjam R Britschgi[1], Hans Acha-Orbea[1], Boris Hinz[2], Jason G Cyster[3] & Sanjiv A Luther[1]

Interleukin 7 is essential for the survival of naive T lymphocytes. Despite its importance, its cellular source in the periphery remains poorly defined. Here we report a critical function for lymph node access in T cell homeostasis and identify T zone fibroblastic reticular cells in these organs as the main source of interleukin 7. *In vitro*, T zone fibroblastic reticular cells were able to prevent the death of naive T lymphocytes but not of B lymphocytes by secreting interleukin 7 and the CCR7 ligand CCL19. Using gene-targeted mice, we demonstrate a nonredundant function for CCL19 in T cell homeostasis. Our data suggest that lymph nodes and T zone fibroblastic reticular cells have a key function in naive CD4$^+$ and CD8$^+$ T cell homeostasis by providing a limited reservoir of survival factors.

After maturing in the thymus, naive T lymphocytes migrate to the periphery, where they continuously recirculate among secondary lymphoid organs (SLOs) such as spleen and lymph nodes. Despite continuous T cell production in the thymus, the number of peripheral T cells remains very constant, indicating that they disappear at the same rate as they are produced in the thymus. It has been proposed that naive T cells compete in the periphery for limiting amounts of survival factors[1–3]. Such homeostatic factors are thought to regulate the maintenance of a diverse T cell repertoire, granting full immunocompetence while preventing the pathology associated with lymphoproliferative disorders or lymphopenia.

Interleukin 7 (IL-7) has been identified as the main factor enhancing naive T cell survival by signaling through the IL-7 receptor α-chain (IL-7Rα) and common γ-chain[1,2,4]. Lack of IL-7 signals due to genetic deficiency or antibody-mediated neutralization induces a gradual loss of peripheral T cells with an approximate half-life of 3 weeks. In contrast, IL-7 overexpression in transgenic mice substantially increases the pool of naive T cells in the periphery. *In vitro*, IL-7 has been shown to keep naive T cells alive that otherwise die within 1–2 d (refs. 1,2). These data indicate that the amount of available IL-7 directly controls the size of the naive T cell pool.

In bone marrow and thymus, IL-7 is produced by stromal cells[4,5]. However, the cell type producing the IL-7 critical for the survival of naive T cells has not been defined[6]. SLOs have been proposed to be the sites at which T cell survival signals are provided. Blockade of the chemokine receptors required for entry into lymph nodes and splenic white pulp cords with the $G\alpha_i$ protein inhibitor pertussis toxin substantially reduces the number of naive T cells present after 1–2 weeks in the total spleen[7]. In lymphopenic conditions, T cells undergo homeostatic proliferation, which has been shown to depend on the presence of intact lymph nodes thought to provide IL-7 and self antigen–major histocompatibility complex signals[8,9]. All these studies have the potential caveat of indirect effects, with pertussis toxin possibly affecting $G\alpha_i$-coupled receptors other than chemokine receptors, and lymph node–deficient mice lacking either nuclear factor-κB–inducing kinase or lymphotoxin-α showing many immune defects. Nevertheless, these observations point to SLOs as a possible source of T cell survival factors.

SLOs are the sites where primary immune responses are initiated[10,11]. The spleen is divided into red and white pulp areas, with the latter being compartmentalized into a B zone (follicles and cortex) and a T zone (paracortex). Lymph nodes consist of B zones and T zones as well as a medullary area for the exit of lymphocytes through the lymphatics. In B zones, B cells are intermingled with stromal cells, such as follicular dendritic cells (FDCs). T zones contain T cells, DCs and a stromal cell type called the 'fibroblastic reticular cell' (FRC). To enter SLOs from the blood, T cells must express several homing molecules, such as the selectin CD62L, the chemokine receptor CCR7 and the integrins $\alpha_4\beta_1$ (VLA-4) and $\alpha_L\beta_2$ (LFA-1). Once they enter, T cells migrate for several hours within the T zone, scanning the environment for DCs presenting their respective antigen. Evidence suggests that this migration is not random but is supported and directed by T zone FRCs[12].

Here we show that blocking access to lymph nodes has deleterious effects on T cell survival similar to those achieved by blocking the IL-7 signal. We identify a population of FRCs positive for glycoprotein gp38 (podoplanin) in the T zone as the main source of IL-7 in SLOs. FRCs are a heterogeneous cell population, with the most prominent

[1]Department of Biochemistry, University of Lausanne, 1066 Epalinges, Switzerland. [2]Laboratory of Cell Biophysics, Ecole Polytechnique Fédérale de Lausanne, 1015 Lausanne, Switzerland. [3]Howard Hughes Medical Institute and Department of Microbiology and Immunology, University of California San Francisco, San Francisco, California 94143-0414, USA. [4]These authors contributed equally to this work. Correspondence should be addressed to S.A.L. (sanjiv.luther@unil.ch).

Received 2 July; accepted 20 August; published online 23 September 2007; doi:10.1038/ni1513

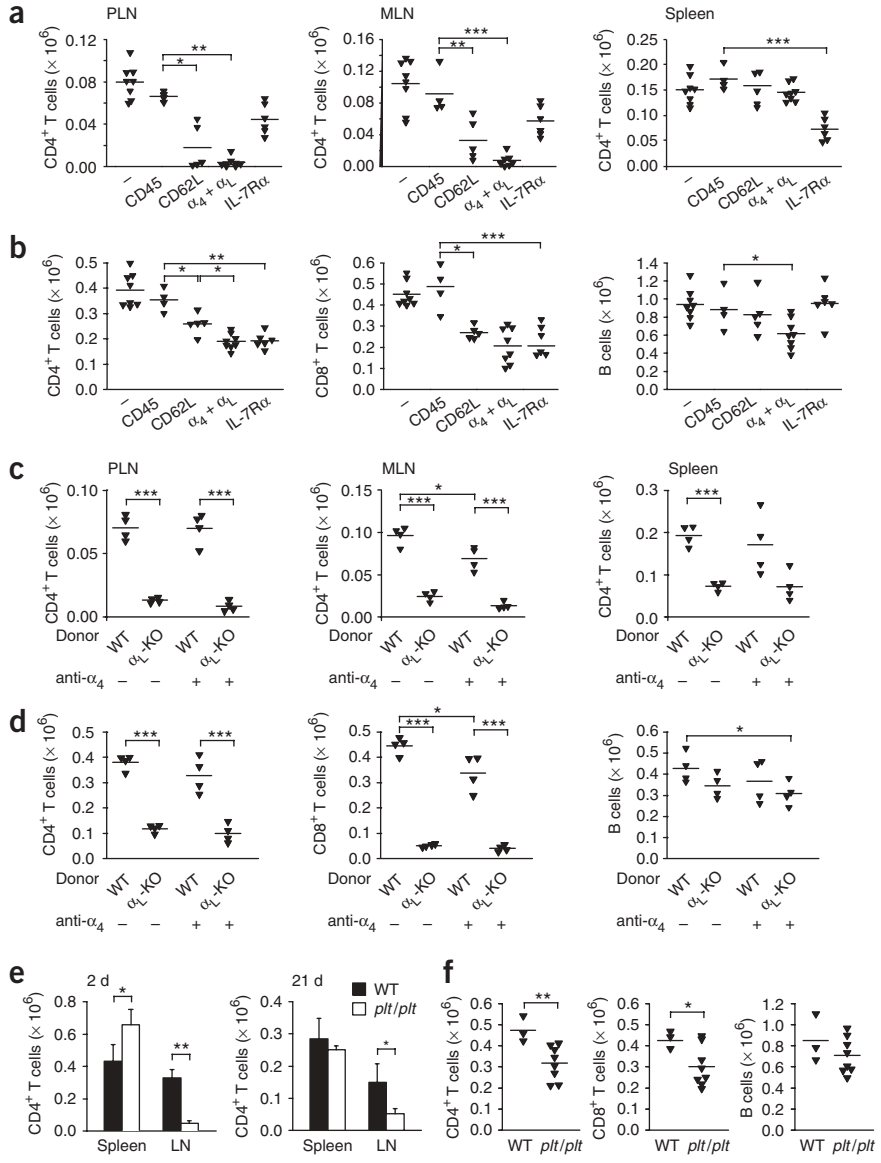

Figure 1 Access to SLOs is important for maintenance of the peripheral T cell pool. (**a**,**b**) Flow cytometry of naive (CD45RB^{hi}) CD45.1$^+$ lymphocytes 3 weeks after adoptive transfer of 25 × 10^6 lymphocytes from CD45.1$^+$ mice into C57BL/6 mice treated every 3 d with 100 μg neutralizing antibodies to CD62L ($n = 5$ mice), α_L and α_4 ($n = 8$ mice), IL-7Rα ($n = 6$ mice), PBS ($n = 8$ mice) or isotype-matched anti-CD45 ($n = 4$ mice). (**c**,**d**) Analysis of lymphocytes from wild-type CD45.1$^+$ mice (WT) and α_L-deficient mice (α_L-KO) transferred together at a ratio of 1:1 into wild-type recipient mice; some recipient mice (anti-α_4 +) were treated with 100 μg neutralizing antibody to α_4. (**a**,**c**) CD4$^+$ T cells in PLN, MLN and spleen. (**b**,**d**) Total CD4$^+$ T cells, CD8$^+$ T cells and B cells (sum of blood, spleen and lymph nodes). (**e**,**f**) CD4$^+$ T cell numbers in spleen and lymph node (LN; MLN + PLN) on days 2 and 21 (**e**) and the sum of CD4$^+$ T cells, CD8$^+$ T cells and B cells in blood, spleen and lymph nodes at day 21 (**f**) after adoptive transfer of CD45.1$^+$ lymphocytes into wild-type C57BL/6 mice ($n = 3$) and *plt*/*plt* mice ($n = 8$). Each symbol represents an individual mouse; small horizontal lines indicate the mean (**a**–**d**,**f**). *, $P < 0.05$; **, $P < 0.01$; ***, $P < 0.001$. Data are representative of three experiments (**a**,**b**,**e**,**f**) or one experiment with four mice per group (**c**,**d**).

subset forming a dense network throughout the T zone and producing the extracellular matrix scaffold of the lymph node[13,14]. We characterize the phenotype of T zone FRCs *ex vivo* and demonstrate their myofibroblast activity. These cells also produced the CCR7 ligands, CCL19 and CCL21, required for T cell recirculation, as suggested before[15]. *In vitro*, T zone FRCs were the only lymph node cell type capable of keeping T cells alive through the secretion of IL-7 and CCL19. In agreement with that finding, CCL19-deficient mice showed defects in naive T cell homeostasis. On the basis of our results, we propose a model for T cell homeostasis in which T zone FRCs have a central function.

RESULTS

Naive T cell homeostasis requires access to SLOs

The entry of naive T cells into lymph nodes can be reduced substantially by blockade of CD62L (L-selectin)[16]. Entry into lymph nodes and partially into splenic white pulp cords can be inhibited by neutralizing antibodies to the integrins α_L (CD11a) and α_4 (CD49d)[17–19]. To determine whether SLOs are involved in the homeostasis of naive T cells, we treated wild-type mice for 3 weeks with neutralizing antibodies to CD62L or to α_L and α_4. To exclude the possibility of thymic effects, we transferred CD45.1$^+$ lymphocytes into CD45.2$^+$ wild-type mice before beginning the antibody treatment. Neutralization of CD62L or of α_L and α_4 led to the expected exclusion of CD4$^+$ and CD8$^+$ T cells from peripheral lymph nodes (PLNs) and mesenteric lymph nodes (MLNs)[16,17,19] (**Fig. 1a** and data not shown). However, T cell numbers in spleen and blood did not increase correspondingly, as might have been expected[16] (**Fig. 1a** and data not shown). Consequently, the total numbers of transferred and endogenous CD4$^+$ and CD8$^+$ T cells recovered after 3 weeks from blood, spleen, PLNs and MLNs were 40–70% less than those of mice treated with a control antibody to CD45 (anti-CD45; **Fig. 1b** and data not shown). The decrease in T cell numbers was slightly greater for mice treated with anti-α_4 and anti-α_L than for mice treated with anti-CD62L, possibly because of the partial blockade of entry into the splenic white pulp cords and mucosal lymphoid tissues by the former treatment[17,18]. Homing to other tissues seems unlikely, as we did not note substantial numbers of CD45.1$^+$ lymphocytes in bone marrow, thymus, liver, lung or gut (data not shown). Notably, there was a similar reduction in transferred and endogenous T cells after treatment of mice with IL-7Rα-neutralizing antibody (**Fig. 1a**,**b** and data not shown). We also recovered significantly fewer B cells from SLOs of mice treated with anti-α_4 and anti-α_L but not from mice treated with anti-IL-7Rα, relative to the recovery of B cells from control mice (**Fig. 1b**).

We used three approaches to rule out the possibility of T cell elimination by antibody-dependent cell-mediated cytotoxicity. First, we injected an isotype-matched control antibody to CD45, which

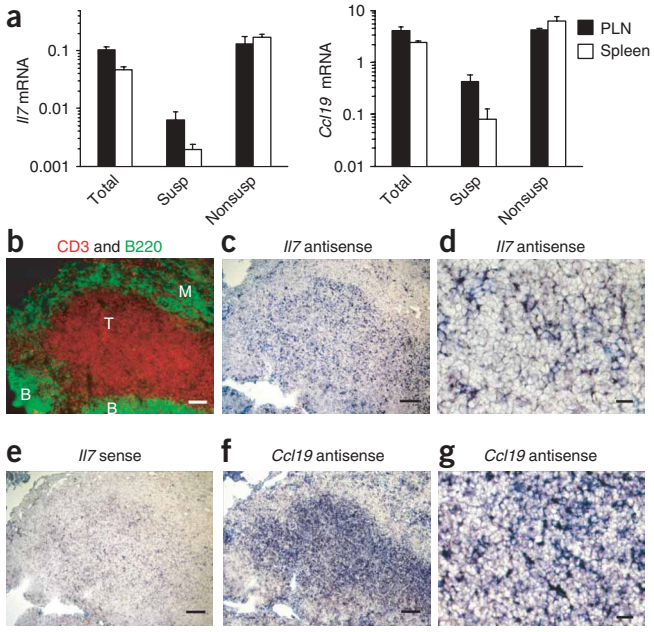

Figure 2 IL-7 is produced mainly in the T zone of SLOs. (**a**) Quantitative RT-PCR of the expression of *Il7* and *Ccl19* mRNA in PLNs and spleens from naive C57BL/6 mice, by analysis of the total organ (Total) or the suspendable fraction (Susp; hematopoietic cells) or nonsuspendable fraction (Nonsusp; stroma) of the organ after mechanical meshing through a cell strainer. (**b**) Immunofluorescence staining of adult PLNs from C57BL/6 mice with anti-CD3 (red) and anti-B220 (green) outlining the T zone (T) and B zones (B), respectively, as well as the medullary cords (M). (**c–g**) *In situ* hybridization analysis of consecutive lymph node sections showing expression of *Il7* and *Ccl19* transcripts selectively in the T cell–rich areas (probes, above images; *Il7* sense probe, negative control). (**d**,**g**) Higher magnification emphasizes the reticular staining pattern in T zones with both the *Il7* and *Ccl19* antisense probes. Scale bars, 100 μm (**b**,**c**,**e**,**f**) or 20 μm (**d**,**g**). Data are representative of one experiment with three independent samples (**a**) or three experiments (**b–g**).

binds most hematopoietic cells; this did not have any effect on T cell survival (**Fig. 1a**,**b**). Second, we labeled wild-type (CD45.1$^+$) and α_L-deficient lymphocytes with CFSE (5-(and 6)-carboxyfluorescein diacetate succinimidyl ester), mixed the cells at a ratio of 1:1 and transferred them into wild-type recipient mice. In this competitive assay, we recovered significantly fewer α_L-deficient CD4$^+$ T cells than wild-type CD4$^+$ T cells from all SLOs and blood (**Fig. 1c** and data not shown). Treatment with anti-α_4 led to blocked lymph node access and a corresponding reduction in total CD4$^+$ T cell numbers only for α_L-deficient but not wild-type CD4$^+$ T cells, indicating that antibody binding did not lead to antibody-dependent cell-mediated cytotoxicity (**Fig. 1c**,**d**). CD8$^+$ T cells showed an even greater dependence on α_L for maintenance of their total peripheral numbers. The numbers of B cells deficient in α_L were significantly reduced only when they were treated with α_4-neutralizing antibodies (**Fig. 1d**). Overall, this approach confirmed the antibody-neutralization experiments described above and showed a greater dependence of T cells on access to SLOs for their survival. In the third approach, we avoided the use of antibodies by transferring wild-type lymphocytes into 'paucity of lymph node T cell' (*plt*/*plt*) mice lacking the chemokine-encoding genes *Ccl19* and *Ccl21-ser*[15,20,21]. On the BALB/c background, these mice have less T cell migration to lymph nodes, leading to higher splenic T cell numbers 2 d after cell transfer, similar to CD62L neutralization[16,20]. We reproduced those findings with *plt*/*plt* mice on the C57BL/6 (B6) background (**Fig. 1e**). At 3 weeks after cell transfer, however, splenic CD4$^+$ T cells returned to wild-type numbers, whereas lymph node exclusion was maintained. As a consequence, the total number of transferred CD4$^+$ and CD8$^+$ T cells, but not B cells, present after 3 weeks in *plt*/*plt* mice was significantly lower (**Fig. 1f**). In summary, we have provided several lines of evidence indicating that the long-term survival of a full repertoire of naive T cells depends on access to lymph nodes and possibly to splenic white pulp cords that may provide limiting amounts of survival factors such as IL-7.

IL-7 is expressed in the T zones of SLOs

Il7 transcripts were easily detectable in extracts of lymph node and spleen (**Fig. 2a**). To determine whether *Il7* was expressed in hematopoietic or stromal cells of lymph nodes and spleens, we used a crude fractionation approach, as described before[15]. For both spleen and PLNs, *Il7* mRNA was strongly enriched in the nonsuspendable stromal fraction, similar to mRNA encoding the chemokines CCL19 (**Fig. 2a**) and CCL21 (data not shown).

IL-7 is reportedly expressed by FDCs in B cell follicles of human tonsils[4,5]. However, by *in situ* hybridization analysis, we detected *Il7* mRNA only in secondary, not primary, B cell follicles (data not shown). Most *Il7* transcripts were in a reticular staining pattern throughout the CD3$^+$ T zone (**Fig. 2b–e**), resembling the expression of *Ccl19* transcripts[15] (**Fig. 2f**,**g**). We also detected transcripts of both *Il7* and *Ccl19* in a reticular pattern in splenic T zones and thymus (data not shown). These data suggest that reticular cells throughout the T zones of SLOs may provide recirculating T cells with the survival factor IL-7.

IL-7 expression by FRCs

The glycoprotein gp38 is a known cell surface marker for FRCs in T zones of SLOs[15,22]. Yet we found expression of gp38 by two other stromal cell subsets in naive PLNs as well: CD35$^+$ FDCs in B cell follicles[14] and lymphatic endothelial cells (LECs) in the medulla that were positive for CD31 and the LEC marker 10.1.1 (**Fig. 3a**). Gp38$^+$CD31$^-$CD35$^-$ FRCs were most abundant in the T zone, but low numbers of these cells were present in other anatomical positions. By light and electron microscopy, four FRC types have been distinguished in rodent lymph nodes: FRCs wrapping around conduits in T zones; 'pericytes' surrounding blood vessels; sinus-crossing cells wrapping around fibers; and sinus-lining cells[13]. Three-color immunofluorescence microscopy with gp38, the lymphoid stroma marker BP-3 (CD157) and CD31 allowed us to distinguish the gp38$^+$ FRC subsets *in situ*. T zone FRCs and pericytes were both BP-3$^+$CD31$^-$, whereas subcapsular sinus-lining cells were BP-3$^+$CD31$^+$ (**Fig. 3a**, **Supplementary Fig. 1a**,**b** online and data not shown). FRCs in the lymph node capsule and gp38$^+$ cells around medullary blood vessels were negative or low for both BP-3 and CD31 (**Supplementary Fig. 1b**,**c** and data not shown). In conclusion, we confirmed the heterogeneity among FRCs based on their location and phenotype. Here we refer to the FRC subset constituting the reticular network in T zones as 'T zone reticular cells' (TRCs).

In cell suspension, where anatomical information is lost, a combination of markers was required for the identification of TRCs. We developed a collagenase-based digestion protocol allowing the isolation and flow cytometric identification of gp38$^+$BP-3$^+$ CD31$^-$ CD35$^-$CD45$^-$ TRCs (**Fig. 3b** and **Supplementary Fig. 1d**). The remaining CD45$^-$ stromal cells were in three main groups: gp38$^+$CD31$^+$ LECs, gp38$^-$CD31$^+$ blood endothelial cells (BECs)[23] and a heterogeneous population of gp38$^-$CD31$^-$ stromal cells. Most

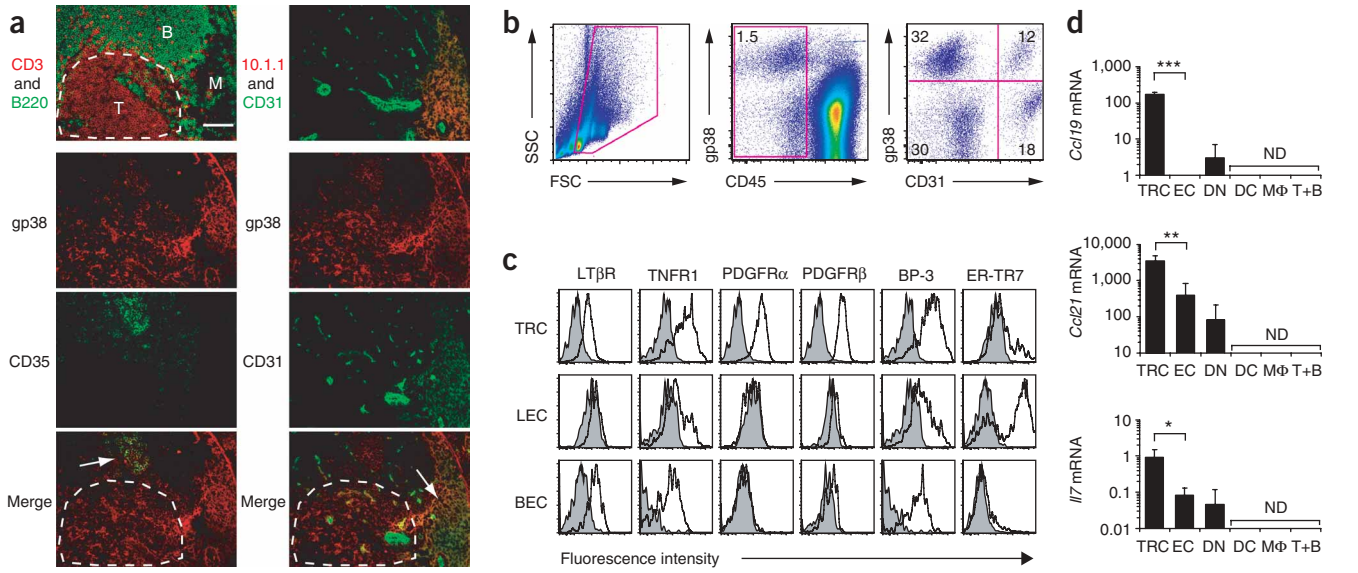

Figure 3 The gp38$^+$CD31$^-$ FRCs are the main source of IL-7 in naive lymph nodes. (**a**) Serial frozen sections of PLNs stained for CD3$^+$ T cells and B220$^+$ B cells or for markers of blood and lymphatic endothelium (CD31), lymphatic endothelium (10.1.1), FRCs (gp38) or FDCs (CD35). Arrows indicate overlapping expression of gp38 with CD35 (FDCs) or CD31 (LECs); dashed line encircles the T zone area where gp38$^+$ staining does not overlap with CD31 or CD35. Scale bar, 100 μm. (**b–d**) Analysis of single-cell suspensions prepared from PLNs by collagenase digestion and stained with anti-CD45, anti-gp38, anti-CD31 and anti-CD35. (**b**) Expression of gp38 and CD31 by CD45$^-$ cells, identifying four stromal cell populations (values below indicate percent of total lymph node cells): TRCs (gp38$^+$CD31$^-$CD35$^-$; 0.45% ± 0.1%); LECs (gp38$^+$CD31$^+$; 0.17% ± 0.04%); BECs (gp38$^-$CD31$^+$; 0.25% ± 0.11%); and double-negative stromal cells (DN; gp38$^-$CD31$^-$; 0.45% ± 0.29%). Number in outlined area (middle) indicates percent CD45$^-$ cells; numbers in quadrants (right) indicate percent cells in each. SSC, side scatter; FSC, forward scatter. (**c**) Expression of additional markers on the surfaces of CD35$^-$ TRCs, LECs and BECs (unshaded), as well as analysis of isotype-matched rat antibody or no primary antibody (negative control; shaded). (**d**) Real-time PCR of the expression of *Ccl19*, *Ccl21* and *Il7* in PLN cell suspensions sorted by flow cytometry into three stromal (CD45$^-$) populations (TRCs; endothelial cells (EC; LECs and BECs) and double-negative (DN)) and by three hematopoietic (CD45$^+$) populations also sorted (CD11c$^+$ DCs; CD11b$^+$ CD11c$^-$ macrophages (MΦ); and CD11b$^-$ CD11c$^-$ cell samples enriched for T cells and B cells (T+B)). ND, not detectable. *, $P < 0.05$; **, $P < 0.01$; ***, $P < 0.001$. Data are representative of at least three independent experiments.

CD35$^+$ cells potentially representing FDCs were among the last population (**Supplementary Fig. 1d**). Consistent with a published report[23], only LECs expressed the lymphatic markers Lyve-1, VEGF-R3 and 10.1.1, whereas BECs showed much higher expression than LECs of VE-cadherin, CD34 and Tie-2 (**Supplementary Table 1** online). TRCs were negative for all those endothelial cell markers but had high expression of both PDGF-Rα and PDGF-Rβ (**Fig. 3c**), suggestive of a mesenchymal cell origin[24]. These cells also expressed the stromal cell markers VCAM-1, ICAM-1 and BP-3, a characteristic they share with FDCs (**Fig. 3c**, **Supplementary Table 1** and **Supplementary Fig. 1a**). The antibody clone ER-TR7, which is widely used as FRC-specific reagent in histology, was not TRC specific by flow cytometry, consistent with its reported extracellular localization in conduits[14,25] (**Fig. 3c** and **Supplementary Fig. 1e**). TRCs stained positive for LTβ-R and TNF-R1 (**Fig. 3c**), which are both 'upstream' regulators of CCL19 and CCL21 (ref. 26). In agreement with that finding, TRCs isolated and sorted from naive lymph nodes were the most abundant source of these chemokines, with at least a tenfold higher expression of *Ccl19* and *Ccl21* mRNA than endothelial cells or gp38$^-$CD31$^-$ stromal cells had. Notably, these cells also had a tenfold more abundant expression of *Il7* mRNA than any other lymph node cell type had (**Fig. 3d**). Hematopoietic cell subsets, including DCs and macrophages, did not show detectable transcripts of *Il7* or the two chemokines, in contrast to reports of human DCs[5]. These data collectively suggest that our protocol allows for the isolation and *ex vivo* characterization of a homogeneous population of TRCs representing the principal source of IL-7, CCL19 and CCL21 in SLOs.

TRCs are myofibroblasts enwrapping conduits

Experiments have suggested that FRCs positive for desmin and α-smooth muscle actin (α-SMA) ensheath extracellular matrix–based microvessels. Such conduits drain fluid and small molecules from the subcapsular sinus to high endothelial venules (HEVs)[12,25,27]. We visualized the conduits by staining with ER-TR7 and subcutaneous injection of Texas red–coupled dextran and confirmed that the surrounding cells corresponded to gp38$^+$ TRCs (**Fig. 4a**). The TRC network is directly connected to a ring of gp38$^+$ pericytes[13,28], a morphologically closely related cell type surrounding the HEVs (**Fig. 4b**). Unexpectedly, most CCL21 was inside the conduit system and not in TRCs themselves (**Fig. 4c**). Despite extensive efforts, we were unable to detect CCL19 and IL-7 by histology, similar to published reports[29]. Transcripts for CCL21 were expressed approximately 200-fold and 3,000-fold more abundantly than those for CCL19 and IL-7, respectively (**Fig. 3d**).

In lymph nodes, coexpression of desmin and α-SMA was specific to gp38$^+$ TRCs (**Fig. 4d**) and pericytes (data not shown), which suggested that TRCs may share certain features with smooth muscle cells or myofibroblasts. Myofibroblasts are smooth muscle–like fibroblasts that have been best described in wound healing and fibrosis, where they exert considerable contractile force[30,31]. In culture, TRCs maintained their gp38$^+$CD31$^-$α-SMA$^+$ desmin-positive phenotype over several days and developed typical myofibroblast morphology (**Supplementary Fig. 1f**). When cultured on thin collagen-coated silicone substrates, they were able to induce wrinkles in the substrate almost as efficiently as lung myofibroblasts, which have a well established contractile function[32]

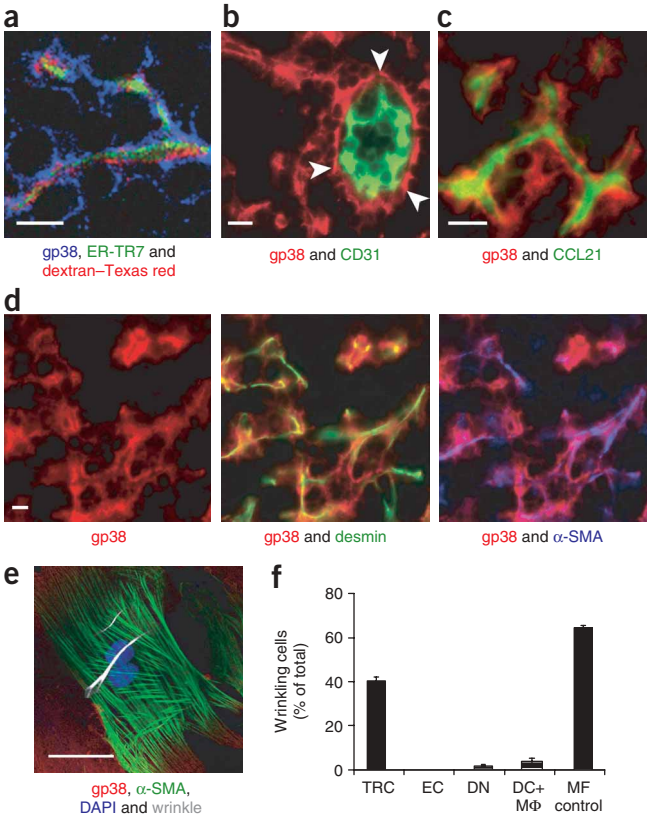

Figure 4 TRCs are myofibroblasts enwrapping conduits. (**a**–**d**) Immunofluorescence microscopy of serial frozen sections of PLNs stained for various markers (below images) for analysis of the T zone. Scale bars, 10 μm. (**a**) The gp38$^+$ TRCs wrap around ER-TR7$^+$ conduits containing subcutaneously injected tracer (dextran–Texas red). (**b**) Pericytes surrounding CD31$^+$ HEVs express gp38 (arrowheads) and connect with the gp38$^+$ TRC network of the T zone. (**c**) The gp38$^+$ TRCs wrap around conduits filled with endogenous CCL21 protein. (**d**) TRCs express both desmin and α-SMA. (**e**,**f**) Contractile properties of PLN cells sorted by flow cytometry into four cell populations (TRCs (CD45$^-$gp38$^+$CD31$^-$), endothelial cells (EC; CD45$^-$CD31$^+$), double-negative cells (DN; CD45$^-$gp38$^-$CD31$^-$) and DCs plus macrophages (DC+MΦ; CD45$^+$ CD11c$^+$ or CD11b$^+$)) and grown for 24 h on collagen-coated silicone substrates, then fixed and immunostained. (**e**) Confocal microscopy showing that only gp38$^+$ TRCs have α-SMA$^+$ stress fibers and develop sufficient tensile force to create wrinkles in the surface of a deformable collagen-coated silicone substrate (white lines in phase-contrast overlay). Cell nuclei are visualized with DAPI (4′,6-diamidino-2-phenylindole dihydrochloride; blue). Scale bar, 20 μm. (**f**) Percent cells in each population that induce wrinkles (three independent samples with over 200 cells per population). MF, lung myofibroblasts of known contractile activity. Data are representative of three experiments (**a**–**e**) or one experiment with three independent samples (**f**).

(**Fig. 4e**,**f**). Other lymph node cell types, such as endothelial cells, gp38$^-$CD31$^-$ stromal cells, DCs and macrophages, were negative for α-SMA and did not contract. These data collectively indicate that TRCs are the main cell subset in naive lymph nodes with myofibroblast features.

TRCs support the survival of naive T cells *in vitro*

To investigate the possible involvement of TRCs in T cell survival, we cultured naive lymphocytes on an adherent layer of lymph node stromal cells containing 30–40% TRCs. The stromal cells considerably enhanced the survival of naive CD4$^+$ and CD8$^+$ T cells (**Fig. 5a**,**b**). This effect was specific to T cells; B cells showed only minimal enhancement of survival (**Fig. 5c**). After 48 h of coculture, 65–80% of the T cells were still alive, compared with only 15–30% without stroma. Between 40% and 50% of T cells survived for more than 7 d and did not change size (forward-scatter profile) or enter the cell cycle, based on Hoechst staining and CFSE dilution (**Fig. 5d** and data not shown). T cells kept their naive phenotype (CD62L^{hi}CD44^{lo}) and were negative for death markers (Trypan blue and 7-amino-actinomycin D; **Supplementary Fig. 1g** and data not shown). They seemed to be still functional after several days of coculture, as they responded to stimulation with anti-CD3 and anti-CD28 by upregulating the activation marker CD69 and by entering cell cycle (data not shown). Sorting of the various stromal cell populations by flow cytometry followed by culture together with purified T cells demonstrated that only TRCs, but no other stromal or hematopoietic cell type in lymph nodes, had a similar ability to keep naive T cells alive (**Fig. 5e**).

The presence of a soluble survival factor was indicated by the observation that CD4$^+$ and CD8$^+$ T cells cultured without physical contact with stromal cells or in medium conditioned by stromal cells survived to almost the same extent as those in direct contact with

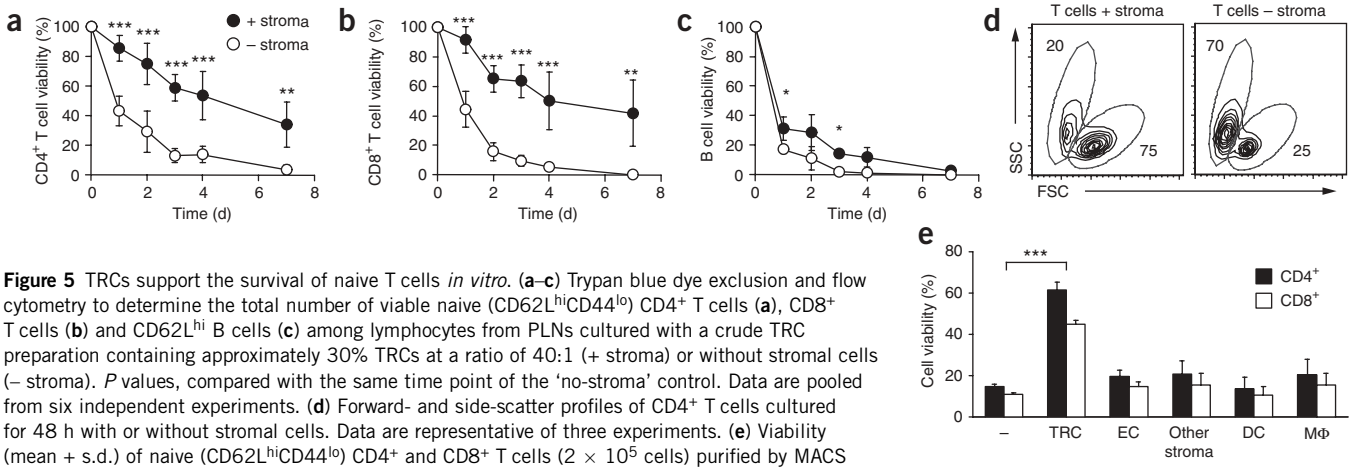

Figure 5 TRCs support the survival of naive T cells *in vitro*. (**a**–**c**) Trypan blue dye exclusion and flow cytometry to determine the total number of viable naive (CD62L^{hi}CD44^{lo}) CD4$^+$ T cells (**a**), CD8$^+$ T cells (**b**) and CD62L^{hi} B cells (**c**) among lymphocytes from PLNs cultured with a crude TRC preparation containing approximately 30% TRCs at a ratio of 40:1 (+ stroma) or without stromal cells (– stroma). *P* values, compared with the same time point of the 'no-stroma' control. Data are pooled from six independent experiments. (**d**) Forward- and side-scatter profiles of CD4$^+$ T cells cultured for 48 h with or without stromal cells. Data are representative of three experiments. (**e**) Viability (mean + s.d.) of naive (CD62L^{hi}CD44^{lo}) CD4$^+$ and CD8$^+$ T cells (2×10^5 cells) purified by MACS and cultured for 48 h with 5×10^3 cells of the following flow cytometry–sorted populations from PLNs: TRCs (CD45$^-$gp38$^+$CD31$^-$CD35$^-$), endothelial cells (CD45$^-$CD31$^+$), other stroma (CD45$^-$gp38$^-$CD31$^-$), DCs (CD45$^+$CD11c$^+$CD11b^{lo}) or macrophages (CD45$^+$CD11b$^+$). Data are representative of three independent experiments. *, $P < 0.05$; **, $P < 0.01$; ***, $P < 0.001$.

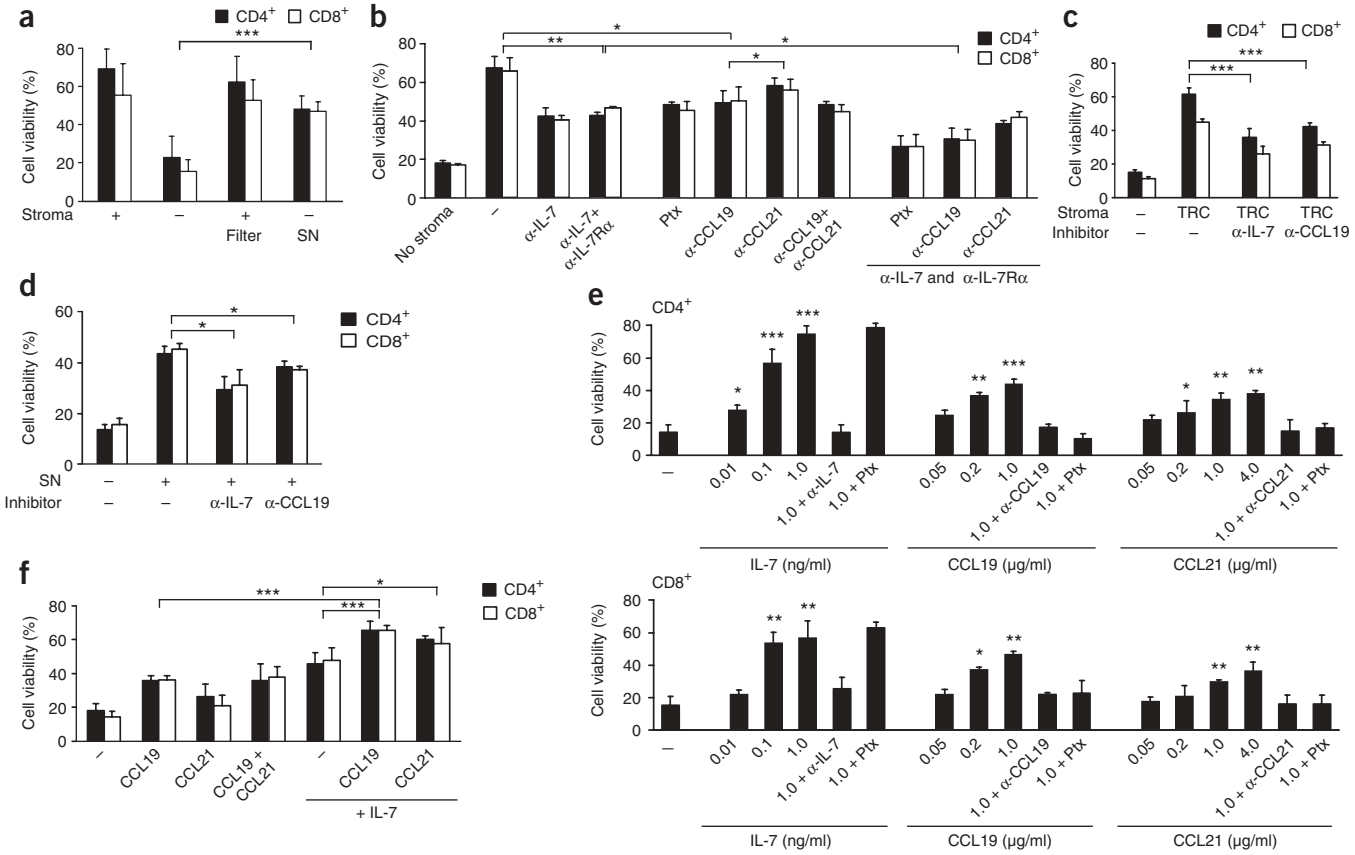

Figure 6 *In vitro*, stromal cells mediate T cell survival by means of IL-7 and CCL19. Trypan blue staining and flow cytometry to assess the viability of naive ($CD62L^{hi}CD44^{lo}$) $CD4^+$ and $CD8^+$ T cells (2×10^5) isolated from PLNs and cultured for 48 h with stromal cells or recombinant proteins. (**a**) T cells cultured in physical contact with subconfluent stromal cells (+), without stroma (–), separated from stromal cells by a transwell filter (Filter) or with stromal cell–conditioned medium (supernatant (SN)). (**b**) T cells purified by MACS and cultured with subconfluent stromal cells in the presence of pertussis toxin (Ptx; 50 ng/ml) or neutralizing antibodies to (α-) IL-7 (10 μg/ml), IL-7Rα (20 μg/ml), CCL19 (10 μg/ml) or CCL21 (20 μg/ml). (**c**) T cells purified by MACS and cultured with flow cytometry–sorted TRCs ($CD45^-gp38^+CD31^-CD35^-$; 5×10^3 cells) in the presence of blocking antibodies to IL-7 or CCL19. (**d**) T cells purified by MACS and cultured in the cell-free supernatants of flow cytometry–sorted TRCs (48 h of conditioning) in the presence of blocking antibodies to IL-7 or CCL19. (**e**) T cells purified by MACS and cultured without stromal cells but in the presence of various concentrations (below bars) of recombinant IL-7, CCL19 or CCL21 plus pertussis toxin or blocking antibodies. *P* values, compared with untreated control. (**f**) T cells purified by MACS and cultured in the presence of a suboptimal concentration of IL-7 (0.1 ng/ml), recombinant CCL19 (0.2 μg/ml), CCL21 (0.2 μg/ml) or combinations thereof. *, $P < 0.05$; **, $P < 0.01$; ***, $P < 0.001$. Data (mean + s.d.) are representative of at least three independent experiments (**a**,**b**,**e**,**f**) or two experiments with three independent samples each (**c**,**d**).

stromal cells (**Fig. 6a**). As expected, IL-7 contributed to this enhanced T cell survival. However, only 50% of the survival effect was abolished by blockade of IL-7 signals (**Fig. 6b**), which suggested the presence of other survival factors. As CCR7 ligands have been proposed to promote DC survival *in vitro*[33], we added pertussis toxin to the coculture to block $G\alpha_i$ protein–coupled receptors. Similar to the IL-7 blockade, T cell survival was reduced by almost half with pertussis toxin or CCL19-neutralizing antibodies (**Fig. 6b**). We confirmed that result in a T cell survival assay with sorted TRCs, consistent with their strong expression of IL-7 and CCL19 (**Fig. 6c**). Neutralization of the second CCR7 ligand, CCL21, had a weak but statistically insignificant effect on stromal cell–induced T cell survival (**Fig. 6b**). We confirmed the absence of cross-reactivity of the chemokine-specific antibodies by chemotaxis assay (**Supplementary Fig. 2a** online). Blocking galectin-1, reported to be involved in T cell survival *in vitro*[34], did not reduce T cell survival mediated by the lymph node stromal cells (**Supplementary Fig. 2b**,**c**). Although IL-7 and CCL19 are probably cell associated or matrix bound *in vivo*[10,35,36], these factors were present in the supernatants of sorted TRCs (**Fig. 6d**). Blocking both CCL19 and IL-7 reduced the survival effect of stromal cells even further (**Fig. 6b**), which suggested that these two factors act in an additive way.

Although recombinant IL-7 is known to keep naive T cells alive *in vitro*, this effect has not been demonstrated for the CCR7 ligands. Both CCL19 and CCL21 were sufficient to enhance naive T cell survival at concentrations similar to those necessary for inducing chemotaxis *in vitro* (**Fig. 6e** and **Supplementary Fig. 2a**). Notably, CCL19 was more potent than CCL21 in mediating survival. Pertussis toxin and chemokine-neutralizing antibodies abolished the effect (**Fig. 6e**). In contrast, the CXCR4 ligand CXCL12 (SDF-1), which also induces T cell chemotaxis, did not have a detectable effect on T cell survival (data not shown). Both CCL19 and CCL21 were able to further enhance the T cell survival mediated by suboptimal doses of IL-7 (**Fig. 6f**). These data collectively suggest that *ex vivo*, TRCs keep naive T cells alive by secreting IL-7 and CCL19.

The generation and characterization of *Ccl19*$^{-/-}$ mice

To investigate the function of CCL19 in naive T cell homeostasis *in vivo*, we generated CCL19-deficient (*Ccl19*$^{-/-}$) mice (**Supplementary**

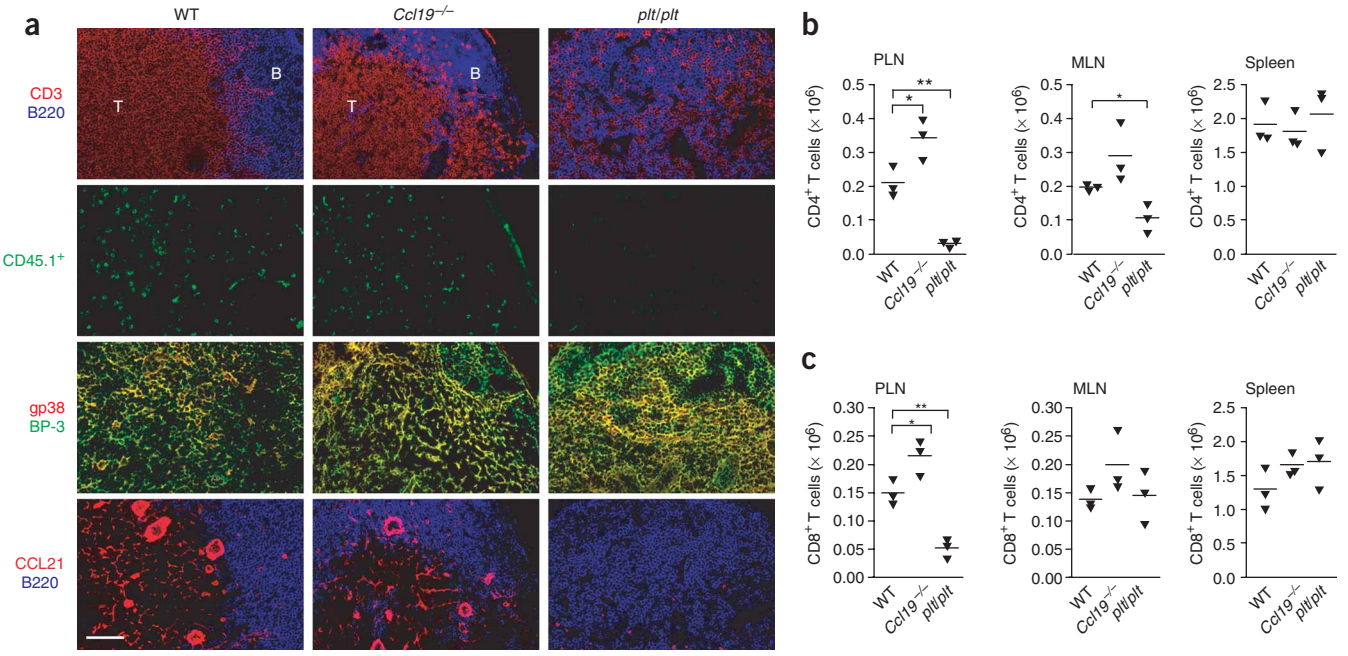

Figure 7 Structure of PLNs and homing of T cells and B cells into SLOs is normal in adult CCL19-deficient mice. Immunofluorescence and flow cytometry to assess the localization and numbers of CD45.1$^+$ T cells and B cells in spleen, lymph nodes and blood at 2 h after adoptive transfer of CD45.1$^+$ lymphocytes into *Ccl19*$^{-/-}$ and *Ccl19*$^{+/+}$ (WT) littermates and *plt*/*plt* mice. (**a**) Immunofluorescence microscopy for various markers (left margin) on consecutive PLN cryosections. Scale bar, 100 μm. (**b**,**c**) Flow cytometry of naive (CD45RB^{hi}) CD45.1$^+$ T cells. Data represent total number of transferred CD4$^+$ (**b**) or CD8$^+$ (**c**) T cells in PLN, MLN or spleen. Each symbol represents an individual mouse; small horizontal lines indicate the mean. *, $P < 0.05$; **, $P < 0.01$. Data are representative of two experiments (**a**) or one experiment (**b**,**c**) with three mice per group.

Fig. 3a,**b** online). These mice lacked detectable expression of CCL19 mRNA and protein in SLOs while maintaining normal expression of the other CCR7 ligand, CCL21 (**Fig. 7a** and **Supplementary Fig. 3c**,**d**). Despite constitutive expression of CCL19 in the thymic medullas of wild-type mice, the architecture and cellular composition of the thymi of adult *Ccl19*$^{-/-}$ mice seemed normal (data not shown). We found that the presence of CCL21 was also sufficient for maintaining normal architecture of lymph nodes and spleen, with segregation of B zones and T zones as well as normal development of stromal cell networks (**Fig. 7a** and **Supplementary Fig. 3e**). Unexpectedly, short-term migration (2 h) of naive T lymphocytes to SLOs also occurred efficiently in *Ccl19*$^{-/-}$ mice. The number of transferred T cells was even higher in lymph nodes (**Fig. 7b**,**c** and **Supplementary Fig. 3e**). In contrast, *plt*/*plt* mice, which are deficient in both CCL19 and CCL21, showed substantial defects in the homing of T cells to T zones, as reported before[20]. In addition, they lacked segregation of B cell and T cell areas, and their TRC networks were considerably compressed (**Fig. 7a** and **Supplementary Fig. 3e**). In summary, CCL19 seems to be dispensable for normal lymphoid tissue architecture and short-term lymphocyte homing. In contrast to *plt*/*plt* mice, CCL19-deficient mice represent an ideal tool for investigating T cell homeostasis in an apparently normal lymphoid environment.

Nonredundant function for CCL19 in T cell homeostasis

Our *in vitro* results suggested that T cell survival may be disturbed in CCL19-deficient mice. Indeed, these mice showed a reduction in total numbers of peripheral CD4$^+$ and CD8$^+$ T cells but not B cells. This reduction seemed to be due to a failure of T cell accumulation in the spleen and blood but not lymph nodes (**Fig. 8a**). To formally exclude the possibility of developmental T cell defects[36], we adoptively transferred wild-type (CD45.1$^+$) cells into *Ccl19*$^{-/-}$ (CD45.2$^+$) mice and determined the total number of transferred lymphocytes in SLOs and blood 3 weeks later. As with endogenous lymphocytes, we recovered significantly fewer transferred T cells but not B cells from *Ccl19*$^{-/-}$ mice than from wild-type mice (**Fig. 8b** and data not shown). This T cell loss was not due to the accumulation of transferred T cells in the bone marrow, thymus, lung, liver or lamina propria of the gut (data not shown).

To obtain an idea of how quickly T cell loss occurred in these organs, we analyzed tissues at various times after the transfer of cells into wild-type or *Ccl19*$^{-/-}$ mice. In *Ccl19*$^{-/-}$ hosts, the transferred CD4$^+$ and CD8$^+$ T cells 'preferentially' accumulated in lymph nodes rather than spleen at all times investigated. However, an equal proportion of T cells was lost from the lymph nodes and spleens of *Ccl19*$^{-/-}$ mice between day 2 and day 21. The total number of peripheral T cells recovered from *Ccl19*$^{-/-}$ hosts decreased gradually and reached 35% below that in control mice after 3 weeks (**Fig. 8c**). In conclusion, CD4$^+$ and CD8$^+$ T cell survival is affected in all SLO types in the absence of CCL19.

The function of CCL19 in naive T cell homeostasis was not as great as that of IL-7, because neutralization of IL-7Rα in wild-type mice led to a reduction of more than 50% in transferred T cells after 3 weeks (**Fig. 8b**). When *Ccl19*$^{-/-}$ mice were treated with IL-7Rα-blocking antibodies, the numbers of transferred T cells recovered were similar to those recovered from treated wild-type mice. These experiments indicate that CCL19 is less important than IL-7 *in vivo* and is not likely to act in an additive way with IL-7 (**Fig. 8b**).

The lower T cell numbers in *Ccl19*$^{-/-}$ mice may be explained by a direct or indirect effect on naive T cell homeostasis. The possibility of a direct effect was indicated by the enhanced T cell survival *in vitro* in the presence of CCL19. However, the non-additive nature of the CCL19 effect *in vivo* led us to consider potential indirect effects of

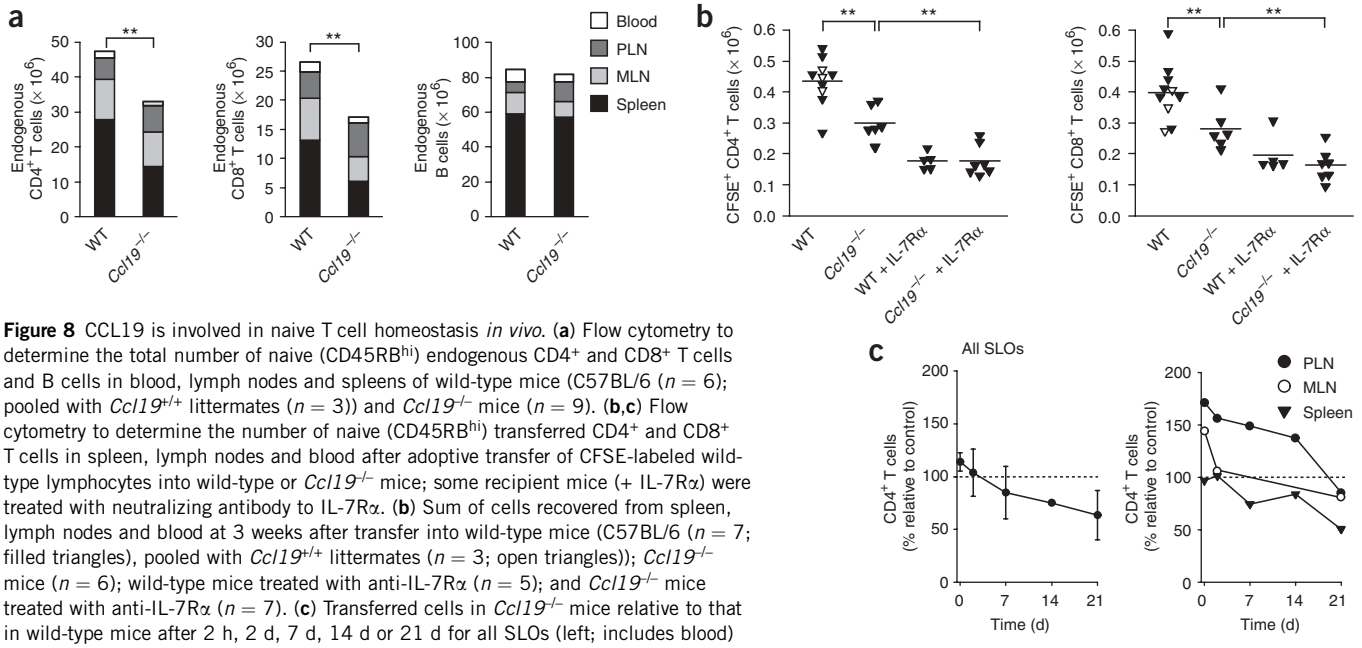

Figure 8 CCL19 is involved in naive T cell homeostasis *in vivo*. (**a**) Flow cytometry to determine the total number of naive (CD45RB^{hi}) endogenous CD4$^+$ and CD8$^+$ T cells and B cells in blood, lymph nodes and spleens of wild-type mice (C57BL/6 ($n = 6$); pooled with *Ccl19*$^{+/+}$ littermates ($n = 3$)) and *Ccl19*$^{-/-}$ mice ($n = 9$). (**b**,**c**) Flow cytometry to determine the number of naive (CD45RB^{hi}) transferred CD4$^+$ and CD8$^+$ T cells in spleen, lymph nodes and blood after adoptive transfer of CFSE-labeled wild-type lymphocytes into wild-type or *Ccl19*$^{-/-}$ mice; some recipient mice (+ IL-7Rα) were treated with neutralizing antibody to IL-7Rα. (**b**) Sum of cells recovered from spleen, lymph nodes and blood at 3 weeks after transfer into wild-type mice (C57BL/6 ($n = 7$; filled triangles), pooled with *Ccl19*$^{+/+}$ littermates ($n = 3$; open triangles)); *Ccl19*$^{-/-}$ mice ($n = 6$); wild-type mice treated with anti-IL-7Rα ($n = 5$); and *Ccl19*$^{-/-}$ mice treated with anti-IL-7Rα ($n = 7$). (**c**) Transferred cells in *Ccl19*$^{-/-}$ mice relative to that in wild-type mice after 2 h, 2 d, 7 d, 14 d or 21 d for all SLOs (left; includes blood) or for each organ separately (right). On days 7 and 14, no MLNs were analyzed. For each time point, three to ten mice were analyzed, except for day 14, with only two mice (no s.d.). Wild-type mice were *Ccl19*$^{+/+}$ littermates. except for day 2, and seven of ten mice for day 21, for which B6J mice were used. **, $P < 0.01$. Data are representative of three experiments (**a**,**b**) or one to four experiments per time point (**c**).

CCL19 on IL-7 function, such as the regulation of its expression, access or signaling. The SLOs of *Ccl19*$^{-/-}$ mice did not show lower abundance of IL-7 transcripts, and naive T cells of *Ccl19*$^{-/-}$ mice did not show lower IL-7Rα expression (**Supplementary Fig. 4a**,**b** online). In addition, expression of the antiapoptosis protein Bcl-2, which is induced by IL-7 survival signals in naive T cells[4,5], was reduced only after IL-7Rα neutralization but not in *Ccl19*$^{-/-}$ mice (**Supplementary Fig. 4c**). In summary, we have provided *in vitro* and *in vivo* evidence for the involvement of TRC-derived CCL19 in T cell homeostasis. The mechanism of CCL19 action *in vivo* still needs to be explored further but does not seem to be mediated by a notable alteration of IL-7 function *in vivo*.

DISCUSSION

Here we have shown that access to lymph nodes is critical for peripheral T cell homeostasis. We found that in lymph nodes, TRCs were the chief source of IL-7 and were able to keep naive T cells alive *in vitro*. TRCs also expressed the chemokines CCL19 and CCL21, which have a similar prosurvival effect *in vitro*. On the basis of our analysis of CCL19-deficient mice, we propose a nonredundant function for CCL19 in the homeostasis of naive T cells.

The involvement of SLO in T cell homeostasis has been indicated by two published reports[7,8]. Here we reinvestigated this issue using nontoxic reagents and by interfering specifically with lymphocyte migration. Short-term inhibition of lymph node entry confirmed the increase in splenic and blood cellularity[19]. When lymph node entry was inhibited for 3 weeks, the number of transferred T cells found in the spleen was no longer increased. This resulted in a considerable reduction in the total peripheral CD4$^+$ and CD8$^+$ T cell pool, confirming and substantially extending results obtained with T cells treated with pertussis toxin[7]. The reduction was comparable to that achieved by blocking the T cell survival signal IL-7 itself. The spleen might therefore provide a limited reservoir of survival factors that is not able to maintain the whole T cell pool over more than a few days. A similar observation has been made before for lymph nodes that keep the same T cell numbers after splenectomy[8], indicating that lymph nodes may also constitute a limited reservoir of T cell survival factors. Consistent with that idea, we found stromal cells in T zones of lymph nodes and spleen to be a chief source of the survival factor IL-7. Access to lymph nodes seemed to be critical for the survival of naive B cells as well. This observation is consistent with the reported expression of the B cell–activation factor BAFF, of the tumor necrosis factor family, in SLOs[37]. These data collectively provide support for the idea that each SLO independently regulates lymphocyte numbers by providing restricted space and limiting amounts of survival factors for which lymphocyte subsets must compete.

We found that TRCs, the main stromal cell population in the T zones of SLOs, produced most of the *Il7* mRNA in uninflamed mouse lymph nodes. We detected less *Il7* in purified endothelial cells, consistent with an observation obtained with human tonsils[38]. The *in situ* localization of *Il7* mRNA, however, resembled more closely the reticular TRC network. In agreement with that finding, TRCs were the only lymph node cell type capable of enhancing naive T cell survival by secreting IL-7 and CCL19. Lymph node stromal cells have been suggested to promote T cell survival, but no function for IL-7 or CCR7 ligands has been found[34,39,40]. CD11b$^+$ stromal cells, presumably macrophages from inflamed lymph nodes, have been shown to mediate survival by producing galectin-1 (refs. 34,39). Although we were able to reproduce the effect of recombinant galectin-1 *in vitro*, we found the TRC-mediated effect to be independent of galectin-1. Another report has shown that mature DCs enhance naive T cell survival in a cell contact–dependent way[40]. In both cases, a 1:1 ratio of T cells to stromal cells was used[39,40], whereas TRCs supported T cell survival at the more physiological ratio of 1 stromal cell to 20–50 T cells. Because of their 'strategic' localization throughout the T zone, we propose that TRCs are the physiological IL-7 source for naive T cells.

A detailed phenotypic and functional characterization of TRCs *ex vivo* has been lacking[13]. Our newly developed isolation and staining protocol allows side-by-side analysis of the main stromal cell types in lymph nodes. A combination of markers was needed for the

identification of TRCs in cell suspension, which were identified by the presence of gp38 and BP-3 and the absence of CD31, CD35 and CD45. This procedure allowed the exclusion of LECs, BECs and subcapsular FRCs from the TRC analysis, in contrast to another report[41]. The resulting TRCs proved to be a distinct and homogeneous stromal cell population, on the basis of analysis of a large panel of surface markers, and were unique in their high expression of CCL19 and CCL21. TRC-like cell lines derived from lymph nodes have been described[14]. However, those cells lack CCL19 and CCL21 expression, presumably because of dedifferentiation during culture over several months. TRCs share properties with myofibroblasts and smooth muscle cells[30,31], as they express both desmin and α-SMA and have the ability to contract. Such features may allow TRCs to contract the conduits and improve fluid movement in these microvessels or to be involved in regulating the plasticity of T zones during the immune response. Because of their unique localization, phenotype and function relative to the three other FRC types[13], we propose that these cells be called 'T zone (fibroblastic) reticular cells'.

T zone stromal cells have been proposed to be the chief source of CCL19 and CCL21 (ref. 15). Here we have provided more direct evidence for that idea by analyzing *ex vivo*–isolated stromal cell subsets and hematopoietic cells. TRCs had tenfold higher expression of CCL21 than did BECs, which include $CCL21^+$ endothelial cells found in HEVs[15]. In that report, some CCL19 expression was noted in splenic $CD8\alpha^+$ DCs but not $CD8\alpha^-$ DCs[15]. Here, in DCs isolated *ex vivo* from lymph nodes, we did not detect *Ccl19* transcripts, consistent with the low frequency of $CD8\alpha^+$ DCs in this tissue. Our observations further strengthen the idea that TRCs (together with HEVs) help induce immune responses in T zones of SLOs by bringing $CCR7^+$ T cells and $CCR7^+$ DCs into physical contact.

Ccr7$^{-/-}$ and *plt*/*plt* mice show aberrant SLO organization because of defective migration of T cells and DC into the T zone[20,21,42]. However, the respective *in vivo* functions of the two CCR7 ligands coexpressed by the same stromal cell type have remained controversial[11,17]. Using CCL19-deficient mice, we have demonstrated here that CCL21 is sufficient for the proper organization of lymphoid T zones and migration of lymphocytes, including transmigration across HEVs. At 2 h after cell transfer into *Ccl19*$^{-/-}$ mice, we noted increased T cell accumulation in lymph nodes, which may have been because of increased sensitivity of the T cells to CCL21. Similarly, *plt*/*plt* T cells transferred into wild-type mice homed more efficiently into lymph nodes[20]. The potential modulation of CCR7 *in vivo* will need further study.

Several lines of evidence suggest CCL19 has a function in regulating T cell homeostasis that cannot be compensated for by CCL21 and that is inferior to the function of IL-7. Recombinant CCL19 or CCL19 produced by TRCs was sufficient to keep T cells alive *in vitro*. Moreover, adult *Ccl19*$^{-/-}$ mice showed a gradual decrease in transferred T cells over time in all SLOs investigated. This defect was also reflected in the reduced number of endogenous T cells. In contrast, the second CCR7 ligand, CCL21, had only a weak effect on T cell survival *in vitro*, consistent with a published report[7]. As lymph nodes and spleen have 100-fold higher expression of CCL21 than of CCL19 (ref. 43), the effects of these ligands *in vivo* may be similar. Results obtained with a transgenic overexpression system have suggested that CCL21 has the potential to induce $CD4^+$ T cell proliferation, at least in a lymphopenic situation[44]. With gene targeting or *plt*/*plt* mice, the effect of CCL21 *in vivo* will be difficult to assess because it is critically involved in the migration of T cells across HEVs[11,20].

CCR7 is reported to induce prosurvival signals in human $CD8^+$ T cells[45] as well as other cell types[46] through the induction of Bcl-2 via the phosphatidylinositol-3-OH kinase–Akt kinase pathway. However, in CCL19-deficient mice, Bcl-2 expression in T cells was not lower, in contrast to the inhibition of IL-7 signals. It is unclear at present what signaling pathways are 'downstream' of CCL19 in mediating this prosurvival effect in T cells or whether they intersect with those induced by IL-7. *In vitro*, IL-7 and CCL19 acted in an additive way, which was not noted in the *in vivo* blocking experiments. It is likely that the context of cytokine presentation and recognition is different in the two situations. *In vivo*, IL-7 and CCL19 are thought to bind to proteoglycans on the TRC surface or in the extracellular space[10,35,36]. In contrast, isolated TRCs have probably been stripped of this extracellular matrix and may only gradually build it up during culture[14], explaining the soluble CCL19 and IL-7 in our assays. So far we have not obtained evidence of an indirect effect of CCL19 on IL-7 expression and recognition *in vivo*. It is possible that the chemokinetic activity of CCL19 (refs. 47,48) influences the quality or quantity of IL-7 signals that T cells receive during their stay in the lymph node.

In summary, we have shown here that lymph nodes and TRCs are key not only in T cell immunity but also in T cell homeostasis. We propose a model in which naive T cells must enter SLOs periodically to access the constitutive but limited reservoir of survival factors produced by TRCs. In the T zone, T cells are physically guided by the three-dimensional TRC network that also supplies them with chemokinetic factors, including CCL19 and CCL21. This perpetual movement in the T zone may allow T cells to compete efficiently for survival factors, such as IL-7, 'posted' on proteoglycans along their path. T cell migration and homeostasis may therefore be linked, and the CCR7 ligands may function in both processes.

METHODS

Mice. C57BL/6 (B6) mice were from Janvier. B6 CD45.1 ($Ly5.1^+$) mice and α_L-deficient (*Itgal*$^{-/-}$) mice were from The Jackson Laboratory. *Ccl19*$^{-/-}$ and *plt*/*plt* mice were backcrossed ten generations to the B6 strain from The Jackson Laboratory, followed by backcrossing for two generations to B6 mice from Janvier. All mice were maintained in pathogen-free conditions. All mouse experiments were authorized by the Swiss Federal Veterinary Office and by the Institutional Animal Care and Use Committee of the University of California San Francisco.

Generation of CCL19-deficient mice. A 9.5-kilobase *Pst*I fragment containing '*Ccl19-atg*' was isolated from a 129 mouse genomic DNA library (Genome Systems) and was then subcloned by means of *Kpn*I to produce a 6.8-kilobase fragment 3′ of *Ccl19-atg*. A targeting vector was constructed in which nucleotides 38–120 of the second exon of *Ccl19-atg* were replaced with an in-frame stop codon followed by a Mengo virus internal ribosomal entry site and the gene encoding enhanced green fluorescent protein and, in the same orientation, a *lox*P-flanked neomycin-resistance gene. The linearized construct was transfected by electroporation into JM1 129/SvJ mouse embryonic stem cells. Aminoglycoside G418–resistant clones were screened by Southern hybridization of *Nco*I-digested genomic DNA to a 0.3-kilobase probe identifying the targeted locus (4 of 300 clones were positive; **Supplementary Fig. 3**), as well as by PCR. Targeted clones were injected into B6 blastocysts. Chimeric males were mated with B6 females and germline transmission of the targeted allele was detected by Southern blot analysis with the 0.3-kilobase internal probe. For removal of the *lox*P-flanked neomycin-resistance cassette, *Ccl19*$^{+/-}$ mice were crossed with mice expressing Cre recombinase under control of the promoter of the gene encoding β-actin, and deletion was verified by PCR. *Ccl19*$^{+/-}$ mice were backcrossed to the B6/J background for at least ten generations. Homozygous mutant mice generated by intercrossing were born at the expected mendelian ratios, were fertile and seemed healthy.

Isolation of TRCs. Peripheral lymph nodes were dissected from mice that had been killed. Capsules of lymph nodes were opened with 26-gauge needles and

lymph nodes were digested for 30 min at 37 °C with gentle stirring in 2 ml RPMI 1640 medium containing collagenase IV (1 mg/ml), DNAse I (40 μg/ml; both from Roche) and 2% (vol/vol) FCS. The remaining fragments were further digested for 20 min at 37 °C with medium containing collagenase D (1 mg/ml) and DNAse I (40 μg/ml). After gentle pipetting, another 2 ml of collagenase D–containing medium was added to the fragments for further incubation. Every 10 min, the suspension was gently pipetted to break up remaining aggregates until no visible fragments remained. During the final pipetting, EDTA was added to a final concentration of 5 mM to further reduce cell aggregates. Cells were then passed through a 40-μm mesh, were washed twice and were resuspended in RPMI 1640 medium containing 10% (vol/vol) FCS. Viable cells were counted by Trypan blue staining before antibody labeling.

T cell survival assay. Single-cell suspensions of digested PLNs were plated at a density of 1×10^6 cells per well in 96-well plates and were incubated at 37 °C in complete RPMI 1640 medium (containing HEPES (10 mM), pH 7.2, penicillin (50 IU/ml), streptomycin (50 μg/ml) and β-mercaptoethanol (50 μM)) with 10% (vol/vol) FBS. Sorted stromal cells were plated at various densities. After 24 h, nonadherent cells were removed by washing of the wells three times with PBS. New medium was added and cells were grown for another 48 h (crude stroma). Then, 2×10^5 total lymphocytes or T cells purified by magnetic-activated cell sorting (MACS) were added to the culture. After various periods of incubation, nonadherent lymphocytes were collected and were stained with antibodies to CD4, CD8, CD19, CD62L and CD44 (**Supplementary Table 2** online). The number of viable lymphocytes was determined by Trypan blue dye exclusion and cells were analyzed with a FACSCanto (Becton Dickinson). The percent surviving cells was calculated based on the total number of viable naive $CD4^+$ and $CD8^+$ T cells ($CD62L^{hi}CD44^{lo}$) and B cells before and after culture.

Flow cytometry and cell sorting. Groups of 1×10^5 to 1.5×10^6 cells were stained in 96-well V-bottomed plates (Falcon). Cells were blocked with 1% (vol/vol) normal mouse serum and were stained with antibodies (**Supplementary Table 2**) in 25 μl PBS containing 2% (vol/vol) FBS, 2 mM EDTA and 0.1% (wt/vol) NaN_3, and were washed twice with 200 μl of this buffer after each step. Unconjugated primary antibodies were detected with secondary reagents (**Supplementary Table 2**). Data were acquired on a FACSCanto (Becton Dickinson) and were analyzed with FlowJo software (TreeStar). For cell sorting, cell suspensions were prepared from PLNs in PBS containing 5% (vol/vol) FCS (Gibco-BRL) and 1 mM EDTA. Cells at a density of 1×10^8 cells per ml were labeled with antibodies and were sorted with a FACSAria (Becton Dickinson).

RNA isolation and quantitative RT-PCR. RNA was extracted with TRIzol reagent (Invitrogen). First-strand cDNA synthesis (Superscript II; Invitrogen) with random nonamer primers (Microsynth) was done according to the manufacturer's instructions. The cDNA was purified with a NucleoSpin Extract II Kit (Macherey-Nagel). A cDNA amount equivalent to 1×10^3 flow cytometry–sorted cells or 3×10^3 cultured cells was amplified with the LightCycler FastStart DNA Master SYBR Green I kit (Roche Diagnostics) on a LightCycler 1.5 (Roche Diagnostics). Efficiency-corrected expression of *Il7*, *Ccl21-ser* and *Ccl19-atg* was normalized by division of that expression with the geometric mean of expression of the 'housekeeping' genes encoding hypoxanthine guanine phosphoribosyl transferase (*Hprt1*) and TATA-binding protein (*Tbp*). Primer sequences (Microsynth) are in **Supplementary Table 3** online.

Purification of T cells by MACS. Cell suspensions were prepared from PLNs by mechanical disruption between glass slides in complete RPMI 1640 medium containing 2% (vol/vol) FBS, then were washed and kept on ice. Non–T cells were labeled with biotin-conjugated antibodies to CD19, CD11b and CD11c (**Supplementary Table 2**), were washed and were incubated at 4 °C with streptavidin microbeads (Miltenyi Biotech). Samples were depleted of labeled cells with an autoMACS (Miltenyi Biotech) according to the manufacturer's instructions, resulting in a T cell purity of over 95%, as determined by flow cytometry.

Adoptive cell transfer. Lymphocytes from the spleens and lymph nodes of $Ly5.1^+$ or B6 mice (25×10^6 cells) were labeled with 20 μM CFSE (Molecular Probes) and were transferred into recipient mice by intravenous injection into the tail vein. For cotransfer experiments, 12.5×10^6 lymphocytes from α_L-deficient (*Itgal*$^{-/-}$) mice and 12.5×10^6 lymphocytes from $Ly5.1^+$ (wild-type) mice were labeled with CFSE, were mixed at a ratio of 1:1 and were adoptively transferred together into wild-type mice. Some mice were injected intraperitoneally every 3 d with 100 μg of neutralizing antibodies to α_L, α_4, IL-7Rα or CD45 (**Supplementary Table 2**); 200 μg was used for anti-CD62L. Then, 3 weeks later, peripheral T cells and B cells were isolated from spleen, lymph nodes and blood, were stained with antibodies to Ly5.1, CD19, CD4 and CD8, CD62L and CD45RB (**Supplementary Table 2**) and were analyzed with a FACSCalibur (Becton Dickinson) for total numbers of transferred $Ly5.1^+$ or $CFSE^+$ cells with a naive phenotype ($CD62L^{hi}CD45RB^{hi}$).

Immunofluorescence microscopy. For visualization of functional conduits, Texas red–labeled dextran (10 kilodaltons; Molecular Probes) was injected subcutaneously into the footpad and mice were killed after 3 min. Lymph nodes were removed soon thereafter and were fixed at 4 °C in 4% (wt/vol) paraformaldehyde and saturated for 3 h at 4 °C in 30% (wt/vol) sucrose before being embedded in Tissue-Tek optimum cutting temperature compound (Sakura), then were frozen in an ethanol dry ice bath. For all other experiments, dissected tissues were embedded in optimum cutting temperature compound (Sakura) without prior fixation. Cryostat sections (8 μm in thickness) on Superfrost/Plus glass slides (Fisher Scientific) were air-dried overnight, then were fixed for 10 min in ice-cold acetone. After rehydration, sections were 'quenched' with 0.3% (vol/vol) H_2O_2, then were blocked with 0.1% (wt/vol) BSA and 1–4% (vol/vol) normal mouse and donkey serum, followed by treatment with a streptavidin-biotin blocking kit (Vector Laboratories). Immunofluorescence staining was done with antibodies (**Supplementary Table 4**) diluted in PBS containing 0.1% (wt/vol) BSA and 1% (vol/vol) normal mouse serum. For gp38 and CCL21, primary antibodies were visualized with biotinylated secondary antibodies and streptavidin–horseradish peroxidase, followed by treatment with the Tyramide Signal Amplification Kit #22 (Molecular Probes) according to the manufacturer's instructions, but with a borate buffer (0.1 M in PBS, pH 8.5) for tyramide dilution. Stromal cells cultured on cover glasses (Fisher Scientific) in six-well cell culture plates (Costar) or on silicone substrates for contraction assays were fixed and stained as reported[32]. Images were acquired on an Axioplan microscope with AxioCam MRm (Zeiss) or on a DM IRE2 microscope with a laser-scanning confocal head TCS SP2 acousto-optical beam splitter (Leica). Confocal images of contraction assays were superposed with transmission confocal images using Adobe Photoshop to highlight the position of wrinkles.

***In situ* hybridization.** The *Il7* 'riboprobe' was cloned as described[49]. Frozen sections (8 μm in thickness) were treated as described[26]. Sections were fixed in 4% (wt/vol) paraformaldehyde, were washed in PBS, were allowed to prehybridize for 1–3 h and were hybridized overnight at 60 °C to sense or antisense digoxigenin-labeled 'riboprobes' in hybridization solution. After being washed at high stringency, sections were incubated with sheep anti-digoxigenin (11333089001; Roche) followed by alkaline phosphatase–coupled donkey anti-sheep (713-055-003; Jackson ImmunoResearch Laboratories) and were developed with nitro blue tetrazolium (Bio-Rad) and 5-bromo-4-chloro-3-indolylphosphate (Sigma).

Wrinkling silicone substrates. Wrinkling silicone elastomer culture substrates for the detection of cell contractile activity were produced with silicone (B.H., unpublished data). Polydimethylsiloxane curing agent and base (Sylgard 184; Dow Corning) were mixed for 3 h at 25 °C at a ratio of between 1:80 and 1:100 (vol/vol)[50] and then were spread onto glass coverslips (Karl Hecht KG) at the bottom of 'home-made' observation chambers to create substrates of about 80 μm in thickness. Substrates were polymerized for 3 d at 25 °C, were sterilized with 70% (vol/vol) ethanol and were coated for 2 h at 37 °C with collagen type I (10 μg/ml; Sigma). The stiffness of these substrates was adjusted to restrict wrinkle formation after 1 d of culture to highly contractile cells, such as mesenchymal cells expressing α-SMA[32].

Statistical analysis. Statistical significance was determined with an unpaired two-tailed Student's *t*-test or one-way analysis of variance followed by a least-significant-difference test. A Levene test for homogeneity of variances was

used to check if the parametric analysis of variance test was appropriate. Elsewhere, an unpaired two-tailed Student's *t*-test for unequal variance was used. For direct comparison of the survival of T cells cultured with or without stroma, statistical significance was calculated with a paired two-tailed Student's *t*-test.

Note: Supplementary information is available on the Nature Immunology website.

ACKNOWLEDGMENTS

We thank M. Ansel, S. Bell, M. Charmoy, T. Andresen, P. Hyman, N. Killeen and J. Smith-Clerc for technical help; H. Robson MacDonald for critical reading of the manuscript; M. Cooper, W. van Ewijk, A. Farr, G. Gabbiani, B. Imhof, C. Ruegg and A. Wilson for antibodies; and N. Killeen for embryonic stem cells. Supported by the Swiss National Science Foundation (PPOOA-68805 to S.A.L.), the Boehringer Ingelheim Fonds (T.K.V.), the Swiss National Science Foundation (3100A0-102150/1 and 3100A0-113733/1 to B.H.) and the National Institutes of Health (AI45073 to J.G.C.).

AUTHOR CONTRIBUTIONS

A.L. did the *in vivo* experiments, with assistance from M.R.B. and S.F., as well as all the *in vitro* assays, flow cytometry sorting and analysis, and *in situ* hybridization, and contributed to the writing of the manuscript; T.K.V. did the wrinkling assays in collaboration with B.H. and did the RT-PCR and assisted with the flow cytometry sorting and analysis; S.F. did most of the immunofluorescence with assistance from T.K.V.; H.A.-O. provided antibodies; S.A.L. generated the CCL19-deficient mice in the laboratory of J.G.C.; S.A.L. directed the study and wrote the manuscript; and all authors critically reviewed the manuscript.

Published online at http://www.nature.com/natureimmunology
Reprints and permissions information is available online at http://npg.nature.com/reprintsandpermissions

1. Marrack, P. & Kappler, J. Control of T cell viability. *Annu. Rev. Immunol.* **22**, 765–787 (2004).
2. Surh, C.D. & Sprent, J. Regulation of mature T cell homeostasis. *Semin. Immunol.* **17**, 183–191 (2005).
3. Freitas, A.A. & Rocha, B. Population biology of lymphocytes: the flight for survival. *Annu. Rev. Immunol.* **18**, 83–111 (2000).
4. Jiang, Q. *et al.* Cell biology of IL-7, a key lymphotrophin. *Cytokine Growth Factor Rev.* **16**, 513–533 (2005).
5. Trinder, P.K. & Maeurer, M.J. in *The Cytokine Handbook* (eds. Thomson, A.W. & Lotze, M.T.) 305–345 (Elsevier Science, London, 2003).
6. Ma, A., Koka, R. & Burkett, P. Diverse functions of IL-2, IL-15, and IL-7 in lymphoid homeostasis. *Annu. Rev. Immunol.* **24**, 657–679 (2006).
7. Cinalli, R.M. *et al.* T cell homeostasis requires G protein-coupled receptor-mediated access to trophic signals that promote growth and inhibit chemotaxis. *Eur. J. Immunol.* **35**, 786–795 (2005).
8. Dai, Z. & Lakkis, F.G. Cutting edge: Secondary lymphoid organs are essential for maintaining the CD4, but not CD8, naive T cell pool. *J. Immunol.* **167**, 6711–6715 (2001).
9. Dummer, W., Ernst, B., LeRoy, E., Lee, D. & Surh, C. Autologous regulation of naive T cell homeostasis within the T cell compartment. *J. Immunol.* **166**, 2460–2468 (2001).
10. Cyster, J.G. Chemokines, sphingosine-1-phosphate, and cell migration in secondary lymphoid organs. *Annu. Rev. Immunol.* **23**, 127–159 (2005).
11. von Andrian, U.H. & Mempel, T.R. Homing and cellular traffic in lymph nodes. *Nat. Rev. Immunol.* **3**, 867–878 (2003).
12. Bajenoff, M. *et al.* Stromal cell networks regulate lymphocyte entry, migration, and territoriality in lymph nodes. *Immunity* **25**, 989–1001 (2006).
13. Gretz, J.E., Anderson, A.O. & Shaw, S. Cords, channels, corridors and conduits: critical architectural elements facilitating cell interactions in the lymph node cortex. *Immunol. Rev.* **156**, 11–24 (1997).
14. Katakai, T., Hara, T., Sugai, M., Gonda, H. & Shimizu, A. Lymph node fibroblastic reticular cells construct the stromal reticulum via contact with lymphocytes. *J. Exp. Med.* **200**, 783–795 (2004).
15. Luther, S.A., Tang, H.L., Hyman, P.L., Farr, A.G. & Cyster, J.G. Coexpression of the chemokines ELC and SLC by T zone stromal cells and deletion of the ELC gene in the plt/plt mouse. *Proc. Natl. Acad. Sci. USA* **97**, 12694–12699 (2000).
16. Lepault, F., Gagnerault, M.C., Faveeuw, C. & Boitard, C. Recirculation, phenotype and functions of lymphocytes in mice treated with monoclonal antibody MEL-14. *Eur. J. Immunol.* **24**, 3106–3112 (1994).
17. Lo, C.G., Xu, Y., Proia, R.L. & Cyster, J.G. Cyclical modulation of sphingosine-1-phosphate receptor 1 surface expression during lymphocyte recirculation and relationship to lymphoid organ transit. *J. Exp. Med.* **201**, 291–301 (2005).
18. Lo, C.G., Lu, T.T. & Cyster, J.G. Integrin-dependence of lymphocyte entry into the splenic white pulp. *J. Exp. Med.* **197**, 353–361 (2003).
19. Berlin-Rufenach, C. *et al.* Lymphocyte migration in lymphocyte function-associated antigen (LFA)-1-deficient mice. *J. Exp. Med.* **189**, 1467–1478 (1999).
20. Nakano, H. *et al.* A novel mutant gene involved in T-lymphocyte-specific homing into peripheral lymphoid organs on mouse chromosome 4. *Blood* **91**, 2886–2895 (1998).
21. Gunn, M.D. *et al.* Mice lacking expression of secondary lymphoid organ chemokine have defects in lymphocyte homing and dendritic cell localization. *J. Exp. Med.* **189**, 451–460 (1999).
22. Farr, A.G. *et al.* Characterization and cloning of a novel glycoprotein expressed by stromal cells in T-dependent areas of peripheral lymphoid tissues. *J. Exp. Med.* **176**, 1477–1482 (1992).
23. Kriehuber, E. *et al.* Isolation and characterization of dermal lymphatic and blood endothelial cells reveal stable and functionally specialized cell lineages. *J. Exp. Med.* **194**, 797–808 (2001).
24. Honda, K. *et al.* Molecular basis for hematopoietic/mesenchymal interaction during initiation of Peyer's patch organogenesis. *J. Exp. Med.* **193**, 621–630 (2001).
25. Sixt, M. *et al.* The conduit system transports soluble antigens from the afferent lymph to resident dendritic cells in the T cell area of the lymph node. *Immunity* **22**, 19–29 (2005).
26. Ngo, V.N. *et al.* Lymphotoxin alpha/beta and tumor necrosis factor are required for stromal cell expression of homing chemokines in B and T cell areas of the spleen. *J. Exp. Med.* **189**, 403–412 (1999).
27. Gretz, J.E., Norbury, C.C., Anderson, A.O., Proudfoot, A.E. & Shaw, S. Lymph-borne chemokines and other low molecular weight molecules reach high endothelial venules via specialized conduits while a functional barrier limits access to the lymphocyte microenvironments in lymph node cortex. *J. Exp. Med.* **192**, 1425–1440 (2000).
28. Bergers, G. & Song, S. The role of pericytes in blood-vessel formation and maintenance. *Neuro. Oncol.* **7**, 452–464 (2005).
29. Mazzucchelli, R. & Durum, S.K. Interleukin-7 receptor expression: intelligent design. *Nat. Rev. Immunol.* **7**, 144–154 (2007).
30. Hinz, B. & Gabbiani, G. Mechanisms of force generation and transmission by myofibroblasts. *Curr. Opin. Biotechnol.* **14**, 538–546 (2003).
31. Gabbiani, G. The myofibroblast in wound healing and fibrocontractive diseases. *J. Pathol.* **200**, 500–503 (2003).
32. Hinz, B., Celetta, G., Tomasek, J.J., Gabbiani, G. & Chaponnier, C. Alpha-smooth muscle actin expression upregulates fibroblast contractile activity. *Mol. Biol. Cell* **12**, 2730–2741 (2001).
33. Sanchez-Sanchez, N. *et al.* Chemokine receptor CCR7 induces intracellular signaling that inhibits apoptosis of mature dendritic cells. *Blood* **104**, 619–625 (2004).
34. Endharti, A.T., Zhou, Y.W., Nakashima, I. & Suzuki, H. Galectin-1 supports survival of naive T cells without promoting cell proliferation. *Eur. J. Immunol.* **35**, 86–97 (2005).
35. Kimura, K. *et al.* Role of glycosaminoglycans in the regulation of T cell proliferation induced by thymic stroma-derived T cell growth factor. *J. Immunol.* **146**, 2618–2624 (1991).
36. Ueno, T. *et al.* Role for CCR7 ligands in the emigration of newly generated T lymphocytes from the neonatal thymus. *Immunity* **16**, 205–218 (2002).
37. Mackay, F. & Ambrose, C. The TNF family members BAFF and APRIL: the growing complexity. *Cytokine Growth Factor Rev.* **14**, 311–324 (2003).
38. Schluns, K.S., Kieper, W.C., Jameson, S.C. & Lefrancois, L. Interleukin-7 mediates the homeostasis of naive and memory CD8 T cells *in vivo*. *Nat. Immunol.* **1**, 426–432 (2000).
39. Zhou, Y.W. *et al.* Murine lymph node-derived stromal cells effectively support survival but induce no activation/proliferation of peripheral resting T cells in vitro. *Immunology* **109**, 496–503 (2003).
40. Feuillet, V., Lucas, B., Di Santo, J.P., Bismuth, G. & Trautmann, A. Multiple survival signals are delivered by dendritic cells to naive $CD4^+$ T cells. *Eur. J. Immunol.* **35**, 2563–2572 (2005).
41. Hara, T. *et al.* A transmembrane chemokine, CXC chemokine ligand 16, expressed by lymph node fibroblastic reticular cells has the potential to regulate T cell migration and adhesion. *Int. Immunol.* **18**, 301–311 (2006).
42. Forster, R. *et al.* CCR7 coordinates the primary immune response by establishing functional microenvironments in secondary lymphoid organs. *Cell* **99**, 23–33 (1999).
43. Luther, S.A. *et al.* Differing activities of homeostatic chemokines CCL19, CCL21, and CXCL12 in lymphocyte and dendritic cell recruitment and lymphoid neogenesis. *J. Immunol.* **169**, 424–433 (2002).
44. Ploix, C., Lo, D. & Carson, M.J. A ligand for the chemokine receptor CCR7 can influence the homeostatic proliferation of CD4 T cells and progression of autoimmunity. *J. Immunol.* **167**, 6724–6730 (2001).
45. Kim, J.W., Ferris, R.L. & Whiteside, T.L. Chemokine C receptor 7 expression and protection of circulating $CD8^+$ T lymphocytes from apoptosis. *Clin. Cancer Res.* **11**, 7901–7910 (2005).
46. Sanchez-Sanchez, N., Riol-Blanco, L. & Rodriguez-Fernandez, J.L. The multiple personalities of the chemokine receptor CCR7 in dendritic cells. *J. Immunol.* **176**, 5153–5159 (2006).
47. Okada, T. & Cyster, J.G. CC chemokine receptor 7 contributes to Gi-dependent T cell motility in the lymph node. *J. Immunol.* **178**, 2973–2978 (2007).
48. Worbs, T., Mempel, T.R., Bolter, J., von Andrian, U.H. & Forster, R. CCR7 ligands stimulate the intranodal motility of T lymphocytes in vivo. *J. Exp. Med.* **204**, 489–495 (2007).
49. Zamisch, M. *et al.* Ontogeny and regulation of IL-7-expressing thymic epithelial cells. *J. Immunol.* **174**, 60–67 (2005).
50. Goffin, J.M. *et al.* Focal adhesion size controls tension-dependent recruitment of α-smooth muscle actin to stress fibers. *J. Cell Biol.* **172**, 259–268 (2006).